RESEARCH PAPERS

Acta Cryst. (1999). A**55**, 783–789

Reverse Monte Carlo modelling of neutron powder diffraction data

A. Mellergård[a]*† and R. L. McGreevy[b]

[a]*Department of Materials Physics, Royal Institute of Technology, S-100 44 Stockholm, Sweden, and* [b]*Studsvik Neutron Research Laboratory, Uppsala University, S-611 82 Nyköping, Sweden. E-mail: anders@matphys.kth.se*

(*Received 25 June 1998; accepted 5 January 1999*)

Abstract

A new reverse Monte Carlo (RMC) method for modelling both lattice and magnetic disorder in powder crystalline materials by direct calculation of the structure factor has been developed. The method, the program and the basic theory are described in some detail. Initial results from modelling the lattice and magnetic structure of MnO around the Néel temperature are also presented.

1. Introduction

For more than 30 years now, the technique of Rietveld refinement has been a valuable tool for modelling the structure of different crystalline systems, based on fitting of powder diffraction data. Recently, modifications of the original ideas have been implemented to allow studies of various systems with increasing disorder. However, one fundamental problem with these techniques is that they mostly concentrate on the Bragg scattering, corresponding to the part of the structure that is still ordered (on a long-range scale) whereas the (local) disorder, which is more directly manifested in the diffuse scattering, is not considered.

On the other hand, RMC modelling techniques have for ten years been used successfully to model the structures of very disordered systems, such as liquids and amorphous materials. These methods, which naturally include diffuse scattering, have been developed for treating less-disordered materials but have so far mainly relied on calculating (C) the model scattering *via* the radial distribution function, $g^C(r)$, and then Fourier transforming to compare with the experimental (E) structure factor, $A^E(Q)$. If used for studies of materials with long-range order, the transform can induce truncation errors; furthermore, it is not always possible to include the instrumental resolution.

A number of ways of overcoming these problems have been suggested. If the system is sufficiently disordered and the experimental Q range is sufficiently large so that all oscillations in the structure factor have died out at the largest Q measured, then $A^E(Q)$ can be transformed directly to $g^E(r)$ without truncation errors and compared with $g^C(r)$ (Keen *et al.*, 1990). However, this procedure is not applicable when there are still oscillations at the maximum experimental Q. The limited Q range and the neglect of the Q variation of the resolution leads to a loss of real-space resolution. If instead we directly transform the model $g^C(r)$ to $A^C(Q)$, for comparison with $A^E(Q)$, we will have truncation errors due to the (finite) size of the RMC model. The radial distribution function, $g_L^C(r)$, of such a model (box length L) is a section of the 'complete' radial distribution function $g^C(r)$, multiplied by a step function $m_L(r)$. $A_L^C(Q)$ is then the convolution of the 'true' structure factor $A^C(Q)$ and the transform of $m_L(r)$, *i.e.* $m_L(Q)$. If the experimental structure factor $A^E(Q)$ is similarly convoluted with $m_L(Q)$ to give $A_L^E(Q)$, then it can be compared directly with $A_L^C(Q)$. While the shape of the structure factor has been modified by the convolution, all the intensity information is maintained, so a quantitative comparison of experiment and simulation can be made (Nield *et al.*, 1992). The problem with this method is that the convolution redistributes errors as well as 'real' data, with an unknown effect. Also, it does not take the resolution into consideration. Another way to avoid the truncation errors is to calculate $g^E(r)$ from $A^E(Q)$ using an inverse method, MCGR (Soper, 1990; McGreevy, 1994; Pusztai & McGreevy, 1997), because $g^E(r)$ can be generated out to any desired r value, hence avoiding truncation. The resolution could in principle be included in the calculation. However, as the Q resolution improves, the required r range also increases ($r_{\max} > 2\pi/\delta Q$, where δQ is the minimum Bragg peak width). This situation would then require an enormous array of $Q \times r$ points, of the order of 10^7 even for medium-resolution powder data, and computer memory becomes a limiting factor (Pusztai & McGreevy, 1997).

All of the above transform methods rely, in a general sense, on 'low resolution' to work and so information is lost. This is not a particular problem for some systems, for example certain fast ion conductors at high

† Present address: Studsvik Neutron Research Laboratory, Uppsala University, S-611 82 Nyköping, Sweden.

temperatures which show few Bragg peaks and much diffuse scattering but, when investigating more ordered systems where Bragg scattering dominates and diffuse scattering is weak, the transform methods are not entirely satisfactory. Instead, a direct calculation of the scattering from the atomic configuration model would be preferred. By choosing the model to be a supercell of the unit cell, both Bragg and diffuse scattering can be calculated in a direct way that avoids truncation errors and includes resolution (Montfrooij *et al.*, 1996). This method is also the basis of RMC modelling of single-crystal diffraction data (Nield *et al.*, 1995; Beverley & Nield, 1997; Proffen & Welberry, 1998). The main disadvantage is that the computer time required per atom move is very large in comparison to that needed for the transform methods.

RMC transform methods have also been used with good results for modelling magnetic structure in amorphous materials (Keen *et al.*, 1995). The present work deals with the possibility of modelling magnetic structure based on powder diffraction data. For these materials, the isotropic spin correlation functions used for amorphous materials are not applicable. We have therefore developed the direct calculation method to include magnetic scattering. Since this increases computer time even more, we have also optimized the basic algorithms.

The report is organized in the following way. First, we discuss the basic expressions for powder diffraction (§§2 and 3). These are included since we calculate the scattering on an absolute scale using theoretical expressions with no arbitrary scaling factors and such expressions are not often given in books or papers. Then we discuss the details of the ideas that are used in the RMC powder program (§4). Finally (§5), we present the first results of using such a direct calculation to simultaneously fit the diffuse and Bragg scattering of both nuclear and magnetic origin as observed in MnO around the Néel temperature.

2. Powder Bragg diffraction

The differential nuclear coherent scattering cross section per atom of a perfect, rigid and infinite single-crystal (cr) containing N atoms per unit cell is (Lovesey, 1984)

$$\mathrm{d}\sigma^{\mathrm{cr}}/\mathrm{d}\Omega = (8\pi^3/NV_{\mathrm{cr}}) \sum_{\boldsymbol{\tau}_{\mathrm{cr}}} |F_N(\mathbf{Q})|^2 \delta(\mathbf{Q} - \boldsymbol{\tau}_{\mathrm{cr}}), \quad (1)$$

where the sum over $\boldsymbol{\tau}_{\mathrm{cr}}$ runs over all allowed vectors of the reciprocal unit cell and V_{cr} is the volume of the crystal unit cell. δ is the Dirac delta function. The lattice structure factor $F_N(Q)$ is defined as a sum over all N atoms in one unit cell by

$$F_N(\mathbf{Q}) = \sum_{j=1}^{N} b_j \exp(i\mathbf{Q} \cdot \mathbf{R}_j), \quad (2)$$

where b_j is the coherent scattering amplitude of atom j and $\mathbf{R}_j$ is its position relative to the origin of the unit cell. To allow for atomic (*e.g.* thermal) displacements, we should extend the summation to all atoms in space. If the displacements are harmonic about equilibrium positions, this procedure leads to the introduction of the familiar Debye–Waller factors in the original expression (2).

For a powder sample, the expression (1) has to be integrated over all orientations of $\boldsymbol{\tau}_{\mathrm{cr}}$. To do this we first note that, for any function $f(\mathbf{Q} \cdot \mathbf{R}_j)$,

$$\int f(\mathbf{Q} \cdot \mathbf{R}_j)\delta(\mathbf{Q} - \boldsymbol{\tau})\, \mathrm{d}\Omega_{\boldsymbol{\tau}} = \int f(\boldsymbol{\tau} \cdot \mathbf{R}_j)\delta(\mathbf{Q} - \boldsymbol{\tau})\, \mathrm{d}\Omega_{\boldsymbol{\tau}}, \quad (3)$$

where $\mathrm{d}\Omega_{\boldsymbol{\tau}} = \sin\theta_{\boldsymbol{\tau}}\, \mathrm{d}\theta_{\boldsymbol{\tau}}\, \mathrm{d}\varphi_{\boldsymbol{\tau}}$. Since the relative orientation of the real and reciprocal lattice is maintained, $\boldsymbol{\tau} \cdot \mathbf{R}_j$ is independent of the integral and

$$\begin{aligned}\int f(\boldsymbol{\tau} \cdot \mathbf{R}_j)\delta(\mathbf{Q} - \boldsymbol{\tau})\, \mathrm{d}\Omega_{\boldsymbol{\tau}} &= f(\boldsymbol{\tau} \cdot \mathbf{R}_j) \int \delta(\mathbf{Q} - \boldsymbol{\tau})\, \mathrm{d}\Omega_{\boldsymbol{\tau}} \\ &= f(\boldsymbol{\tau} \cdot \mathbf{R}_j)\, \delta(Q - \tau)/\tau^2, \quad (4)\end{aligned}$$

where the last equality is obtained by the variable transformation

$$\begin{aligned}(\tau, \theta_\tau, \varphi_\tau) &\rightarrow (\tau_x, \tau_y, \tau_z) \\ &= (\tau \sin\theta_\tau \cos\varphi_\tau, \tau \sin\theta_\tau \sin\varphi_\tau, \tau \cos\theta_\tau). \quad (5)\end{aligned}$$

Thus, for the powder (pow) cross section

$$\begin{aligned}\mathrm{d}\sigma^{\mathrm{pow}}/\mathrm{d}\Omega &= (1/4\pi) \int (\mathrm{d}\sigma^{\mathrm{cr}}/\mathrm{d}\Omega)\, \mathrm{d}\Omega_{\boldsymbol{\tau}} \\ &= (2\pi^2/NV_{\mathrm{cr}}) \sum_{\boldsymbol{\tau}_{\mathrm{cr}}} |F_N(\boldsymbol{\tau}_{\mathrm{cr}})|^2\, \delta(Q - \tau_{\mathrm{cr}})/\tau_{\mathrm{cr}}^2. \quad (6)\end{aligned}$$

In real experiments, the delta function is of course replaced by the instrument resolution function.

For magnetic scattering, we have instead the single-crystal cross section (Lovesey, 1984)

$$\mathrm{d}\sigma_M^{\mathrm{cr}}/\mathrm{d}\Omega = [r_0^2(2\pi)^3/NV_{\mathrm{cr}}] \sum_{\boldsymbol{\tau}_{\mathrm{cr}}} |F_M(\mathbf{Q})|^2 \delta(\mathbf{Q} - \boldsymbol{\tau}_{\mathrm{cr}}), \quad (7)$$

where $r_0 = \gamma_n e^2/(4\pi\varepsilon_0 m_e c^2) = -5.391$ fm is the product of the neutron gyromagnetic ratio and the classical electron radius. The magnetic structure factor is given by

$$\begin{aligned}|F_M(\mathbf{Q})|^2 = \Big| &\sum_j \tfrac{1}{2} g_j \langle S_j \rangle f_j^m(\mathbf{Q}) \exp(i\mathbf{Q} \cdot \mathbf{R}_j) \\ &\times \left[\widehat{\mathbf{Q}} \times \left(\widehat{\boldsymbol{\mu}}_j \times \widehat{\mathbf{Q}}\right)\right]\Big|^2. \quad (8)\end{aligned}$$

Here, g_j, S_j and $f_j^m(\mathbf{Q})$ are the Landé factor, total spin and magnetic form factor, respectively, of spin j. Defining an effective moment as $p_j = g_j \langle S_j \rangle$ and using the vector identity

$$\begin{aligned}&\left[\widehat{\mathbf{Q}}\times\left(\widehat{\boldsymbol{\mu}}_i\times\widehat{\mathbf{Q}}\right)\right]\cdot\left[\widehat{\mathbf{Q}}\times\left(\widehat{\boldsymbol{\mu}}_j\times\widehat{\mathbf{Q}}\right)\right]\\&\quad=\widehat{\boldsymbol{\mu}}_i\cdot\widehat{\boldsymbol{\mu}}_j-\left(\widehat{\mathbf{Q}}\cdot\widehat{\boldsymbol{\mu}}_i\right)\left(\widehat{\mathbf{Q}}\cdot\widehat{\boldsymbol{\mu}}_j\right),\end{aligned}\tag{9}$$

we have

$$\begin{aligned}|F_M(\mathbf{Q})|^2=&\sum_{\alpha=x,y,z}\left|\sum_j\widehat{\boldsymbol{\mu}}_{j\alpha}[p_jf_j^m(\mathbf{Q})/2]\exp(i\mathbf{Q}\cdot\mathbf{R}_j)\right|^2\\&-\left|\sum_j\left(\widehat{\mathbf{Q}}\cdot\widehat{\boldsymbol{\mu}}_j\right)[p_jf_j^m(\mathbf{Q})/2]\exp(i\mathbf{Q}\cdot\mathbf{R}_j)\right|^2.\end{aligned}\tag{10}$$

If there is only one type of spin, then $p_j=p$ and $f_j^m(\mathbf{Q})=f^m(\mathbf{Q})$. Introducing

$$\begin{aligned}F_{M\alpha}(\mathbf{Q})&=\sum_j\widehat{\boldsymbol{\mu}}_{j\alpha}\exp(i\mathbf{Q}\cdot\mathbf{R}_j),\quad\alpha=x,\,y,\,z,\\F_{MQ}(\mathbf{Q})&=\sum_j\left(\widehat{\mathbf{Q}}\cdot\widehat{\boldsymbol{\mu}}_j\right)\exp(i\mathbf{Q}\cdot\mathbf{R}_j),\end{aligned}\tag{11}$$

we can now write the magnetic structure factor as

$$|F_M(\mathbf{Q})|^2=|pf^m(\mathbf{Q})/2|^2\Big[\sum_{\alpha=x,y,z}|F_{M\alpha}(\mathbf{Q})|^2-|F_{MQ}(\mathbf{Q})|^2\Big].\tag{12}$$

Integrating over all orientations of $\boldsymbol{\tau}$, we finally obtain

$$\begin{aligned}\mathrm{d}\sigma_M^{\mathrm{pow}}/\mathrm{d}\Omega=&(2\pi^2/NV_{\mathrm{cr}})(r_0\,p/2)^2\sum_{\boldsymbol{\tau}_{\mathrm{cr}}}|f^m(\boldsymbol{\tau}_{\mathrm{cr}})|^2\\&\times[\delta(Q-\tau_{\mathrm{cr}})/\tau_{\mathrm{cr}}^2]\\&\times\Big[\sum_{\alpha=x,y,z}|F_{M\alpha}(\boldsymbol{\tau}_{\mathrm{cr}})|^2-|F_{MQ}(\boldsymbol{\tau}_{\mathrm{cr}})|^2\Big].\end{aligned}\tag{13}$$

3. Diffuse scattering

So far we have derived the expressions for the elastic Bragg scattering of a powder sample. Consider now a model consisting of $N_a\times N_b\times N_c$ crystal unit cells, *i.e.* a supercell (sc) of the crystal unit cell, with periodic boundary conditions. The scattering from such a model would be described by the reciprocal-lattice vectors of the supercell, $\boldsymbol{\tau}_{\mathrm{sc}}$, substituted into the expressions (6) and (13) above. With all atoms at equilibrium crystal positions, scattering will only be observed at the Bragg peaks of the crystal unit cell, $\boldsymbol{\tau}_{\mathrm{cr}}$, which are a subset of $\boldsymbol{\tau}_{\mathrm{sc}}$. When disorder is introduced into the model, by atomic displacements and spin rotations, intensity will start to build up in other peaks as well. These peaks are effectively the diffuse scattering of the (now disordered) model crystal. In the limit of infinitely large models, the periodic boundary conditions will become irrelevant and the model scattering will approach that of a real sample including diffuse features. For a finite model, we must, in practice, make some approximations so that the 'additional' Bragg peaks from the supercell (*i.e.* those that are not peaks of the crystal unit cell) can be used to represent the diffuse scattering. The methods used will be explained in detail below.

4. The powder RMC technique

The supercell approach to calculate diffuse scattering corresponds to a partition of reciprocal space into equal size cells around each $\boldsymbol{\tau}_{\mathrm{sc}}$. Each cell contributes one term (peak) in the scattering cross section. To improve the ability of a finite model to reproduce the experimentally observed diffuse scattering, we can average the intensity of each peak over the reciprocal volume of the cell it occupies. This procedure can be performed in one dimension (for powder data) by smoothing the intensity of each diffuse peak over the equivalent linear Q extension of the cell. Furthermore, the total number of diffuse peaks that have to be calculated can be greatly reduced by grouping neighbouring cells together and then calculating the average contribution of this volume.

The volume in reciprocal space of one allowed $\boldsymbol{\tau}_{\mathrm{sc}}$ is $V_{\mathrm{sc}}^*=8\pi^3/V_{\mathrm{sc}}$, where the volume of the supercell is $V_{\mathrm{sc}}=N_aN_bN_cV_{\mathrm{cr}}$. If the maximum Q measured in the experiment is $Q_{\max}$, then the number of supercell peaks with $Q<Q_{\max}$ is

$$N_{\boldsymbol{\tau}}(Q_{\max})=\frac{4\pi Q_{\max}^3/3}{8\pi^3/V_{\mathrm{sc}}}=\frac{V_{\mathrm{sc}}Q_{\max}^3}{6\pi^2}.\tag{14}$$

A typical model configuration might consist of 8000 atoms with an atomic density of $0.08\ \text{Å}^{-3}$, so that $V_{\mathrm{sc}}\simeq10^5\ \text{Å}^3$ (*i.e.* the linear dimension is $\sim$50 Å). On reactor-based diffractometers, $Q_{\max}\simeq10\ \text{Å}^{-1}$, giving $N_{\boldsymbol{\tau}}\simeq2\times10^6$. If inversion symmetry of the reciprocal lattice is applicable (as is usually the case), then we only have to calculate peaks in one half of the reciprocal space. $N_{\boldsymbol{\tau}}$ is then reduced by a factor of 2, but it is still too large for practical computing.

Assuming that the intensity from neighbouring $\boldsymbol{\tau}_{\mathrm{sc}}$ vectors in the diffuse part varies smoothly, we can average over *e.g.* $2\times2\times2$ $\boldsymbol{\tau}_{\mathrm{sc}}$ cells using only the central peak in this volume, with the intensity multiplied by eight. This reduces the total number of diffuse peaks by a factor of eight, but we will have a very low density of peaks (in a linear sense) at low Q. To avoid this, we note that for low Q the accumulated number of $\boldsymbol{\tau}_{\mathrm{sc}}$ vectors is (relatively) small since $N_{\boldsymbol{\tau}}\simeq Q^3$. Thus we can keep all peaks at low Q by dividing the reciprocal space in two regions, as illustrated in Fig. 1. Dashed lines show the partition of reciprocal space. Bragg peaks, $\boldsymbol{\tau}_{\mathrm{cr}}$, are marked by dots. In the inner part, we use all diffuse peaks whereas, in the outer part, we only use each eighth as described above. Note that both the inner and the outer region will contribute to the intensity for $Q_1<Q<Q_2$. Using $Q_1=3\ \text{Å}^{-1}$ for the typical model above, there are now only 1.5×10^5 peaks to be calculated (including also inversion-symmetry reduction). This is now computationally practical.

The split of the Q region has to be made with some care. Firstly, there are a small number of special cases at the interface which are accounted for in the program but are not discussed here. Secondly, the volume around the Bragg peaks in the high-Q region must be treated separately, as shown in Fig. 2(a). Open circles represent the allowed $\boldsymbol{\tau}_{\rm sc}$ values of the supercell. Here $N_a = N_b = 6$ and so Bragg peaks correspond to the filled circles. Dashed lines denote the 2×2 cells which are centred at multiples of two in each $\boldsymbol{\tau}_{\rm sc}$ index. Since the central peaks indicated by filled circles are used for the 1×1 cells of Bragg peaks, we cannot use them for the surrounding diffuse-cell average. With no further corrections, we would therefore lose diffuse intensity corresponding to the shaded area. In three dimensions, there will be in total $(2^{-3}N_aN_bN_c - 1) + (2^3 - 1)$ missing diffuse peaks, so this can give a considerable loss of calculated intensity.

In the current version of the code, we instead displace the averaging regions by one index unit in each direction, as in Fig. 2(b), so that we obtain an overlap of Bragg and diffuse cells in the dotted regions. Then we have only one extra diffuse peak per Bragg peak. Note that these partitions restrict the supercell to be an *even* number of crystal unit cells in each direction. Variations of the $2 \times 2 \times 2$ scheme might be used if other multiples of unit cells are preferred (*e.g.* in the case of some particular tendency for the formation of a magnetic supercell). In principle, the contribution from the neighbouring diffuse cells could be subtracted from the corresponding Bragg cells. However, this is computationally relatively expensive, since it involves 'special cases', and so has not been included.

The first step in smoothing the diffuse intensities is to group them into the appropriate Q bins of the experimental data. Owing to the sampling at discrete **Q** vectors, the diffuse scattering appears rather wavy at this stage. Since we are assuming that diffuse intensities vary smoothly in between supercell reciprocal vectors, we can then smear out the scattering using an averaging algorithm. Originally, we applied a simple moving-average procedure but later we found that the cubic smoothing algorithm proposed by Savitzky & Golay (1964) was better suited for this operation. A natural choice for the length scale of the smoothing interval is then the approximate distance between neighbouring crystal Bragg peaks, given by $\Delta Q = (V^*_{\rm cr})^{1/3}$. In the MnO study reported below, this length was found to give good results, but more complicated systems might need shorter smoothing intervals. It should be pointed out that with the linear-smoothing approach we neglect the possible variation of ΔQ with respect to the three lattice

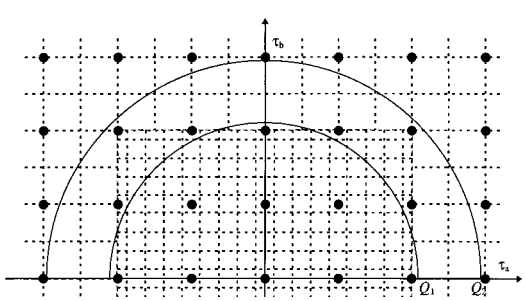

Fig. 1. Half-plane of a two-dimensional reciprocal lattice showing the partition of cells in reciprocal space at low and high Q. $N_a = N_b = 4$, Filled circles correspond to Bragg peaks. If $|\boldsymbol{\tau}_a|$ and $|\boldsymbol{\tau}_b|$ are both less than Q_1, all diffuse peaks, which are at the centres of the 1×1 dashed cells, are used. If either $|\boldsymbol{\tau}_a|$ or $|\boldsymbol{\tau}_b|$ is greater than Q_1, the central diffuse peaks of the 2×2 cells are averaged over the 2×2 dashed cells. Q_2 denotes the maximum linear **Q** value for which the inner region contributes to the scattered intensity.

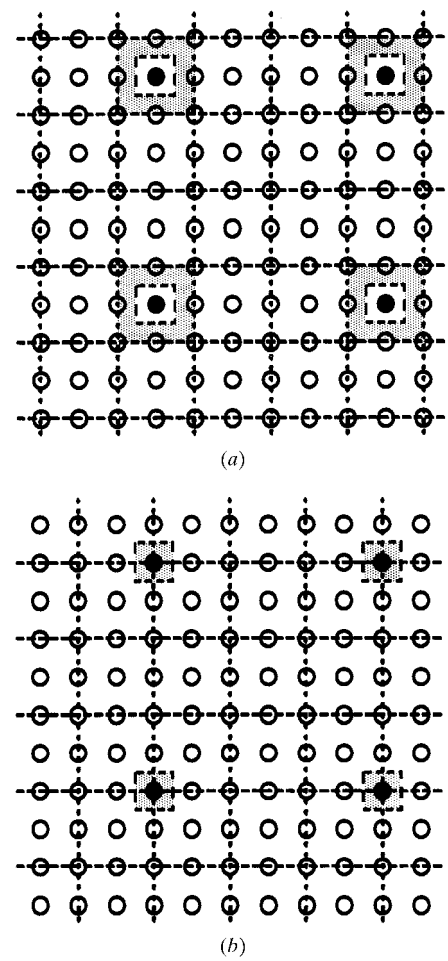

Fig. 2. Sections of a 6×6 supercell reciprocal lattice. Open circles correspond to supercell peaks, $\boldsymbol{\tau}_{\rm sc}$. Filled circles corrrespond to Bragg peaks, $\boldsymbol{\tau}_{\rm cr}$. Dashed lines show the partition into 1×1 cells for the Bragg peaks and 2×2 cells for averaging the diffuse scattering using the central peak of each such cell, as described in the text. (a) Diffuse cells are centred at multiples of two in each $\boldsymbol{\tau}$ index. Shaded areas represent regions not covered by Bragg or diffuse cells. (b) Diffuse cells are displaced one unit in each $\boldsymbol{\tau}$ index. Here Bragg and diffuse cells overlap in the shaded areas.

directions. If we use models with similar sizes in all directions, by choosing appropriate values of N_a, N_b and N_c, then the supercell reciprocal lattice becomes approximately cubic and this effect is of minor importance.

In standard RMC and MCGR methods, the pair distribution function is used for intermediate results. In the program *RMCPOW*, the basic units to store and update after each atom/spin move are obviously the lattice and magnetic scattering amplitude sums given by equations (2) and (11), for each $\boldsymbol{\tau}_{sc}$. As can be seen from (11), there are actually four magnetic sums, namely F_{M_α}, with $\alpha = x, y, z$, and F_{MQ}. From these the total structure factor can be calculated using (6) and (13). Updating these sums after an atom move or a spin rotation only involves the change for one atom/spin (for each $\boldsymbol{\tau}_{sc}$), whereas initially the sums have to be calculated for all atoms/spins in the configuration.

Finally, the resolution is easily applied by first calculating the intensities from the amplitude sums of (2) and (11) for each $\boldsymbol{\tau}_{sc}$ and then convoluting them with the resolution function. This is just a normalized distribution which could be any of the standard powder line shapes. In the present work, a simple Gaussian distribution was used. Since lattice and resolution parameters are kept fixed, the resolution function needs to be calculated only at the beginning of the program. This should, in principle, be performed for each $\boldsymbol{\tau}_{sc}$, but to save computer time and memory only the Bragg peak shapes are calculated individually. Because of its broad character, the diffuse intensity can be convoluted after summing regions and smoothing, and so only needs the resolution as a function of Q for each experimental Q bin.

The ideas described above have been implemented in the program *RMCPOW*, which can model the lattice and/or magnetic structure (at present only one type of magnetic species) of a crystal based on fitting to powder diffraction data, including both Bragg and diffuse scattering. It should be emphasized that the data must be absolutely normalized and properly corrected for all background scattering, *etc*. (this is rarely ever performed). The current version needs the lattice parameters of the crystal cell and the resolution parameters as input, so initial Rietveld refinement of the Bragg scattering is required. The effective moment p is fixed, but may be adjustable in the future. The compiled version of the code, which can deal with up to 10^6 peaks, uses 10 Mbyte of RAM memory on a DEC Alpha computer. For a model the size of that used for MnO, as described below, the average calculation time for one move is ~2 s with magnetic scattering included. Without magnetic scattering, the time is ~0.5 s. With a sensible starting configuration (complementary programs to set up ordered or partially disordered configurations of various symmetries are available), we have found that about 50 000 moves seem to be needed for convergence; thus the total computing time is below 24 h.

5. Application to neutron scattering from MnO

To test the *RMCPOW* program, we have measured $A(Q) \equiv \mathrm{d}\sigma^{\mathrm{pow}}/\mathrm{d}\Omega$ for MnO at a number of temperatures between 15 and 1100 K, using the SLAD diffractometer at the Studsvik Neutron Research Laboratory. Herein, only a preliminary study of the 15 and 200 K data sets is discussed. This 'simple' magnetic system, having a large effective spin number, offers the possibility of studying the development of magnetic diffuse scattering around the Néel temperature, $T_N = 120$ K, as can be seen in Fig. 3. The crystal structure is similar to that of rock salt but has a small rhombohedral distortion below and just above T_N. Mn spins order in ferromagnetic sheets parallel to (111) with alternating direction of magnetization of consecutive sheets (Roth, 1958).

The lattice parameters and Debye–Waller factors were obtained by Rietveld refinement using the corresponding hexagonal unit cell needed to describe the enlarged magnetic crystal cell. For convenience, this was also used in the RMC model. The initial models, consisting of $6 \times 6 \times 4$ such cells (6912 atoms and 3456 spins), were produced by applying Gaussian-distributed random displacements, given by the Rietveld-refined thermal factors, to the equilibrium lattice at the appropriate temperature. Starting from completely ordered spin configurations, magnetic disorder was initially introduced by random rotations of all spins within a given maximum angle (30° for 15 K and 80° for 200 K data). This was estimated on the basis of the expected spin disorder as observed by Rietveld refinement. For both temperatures, the diffraction patterns of the initial models turned out to be inconsistent with the experimental data, giving approximately correct reduction of Bragg scattering intensity but only paramagnetic diffuse scattering. In fact, it is clear, since there are peaks in the experimental diffuse scattering at nonzero Q, that the

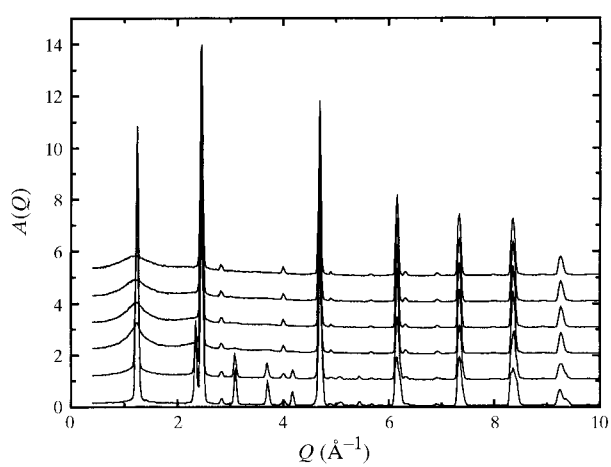

Fig. 3. $A(Q)$ for MnO at, in ascending order, 15, 100, 120, 130, 150 and 200 K. Each data set is offset vertically by one unit for clarity.

magnetic disorder is not due to simple uncorrelated spin rotations. Even at 15 K there is still significant magnetic diffuse scattering, so the system is not completely ordered. The model scattering was calculated using low- and high-Q regions as described above, with $Q_1 = 2.5$ Å^{-1}. Both temperatures were modelled using some 50 000 accepted atom moves and 30 000 spin rotations, after which no further improvement in the fit was found.

The 200 K data show good agreement of the experimental and calculated scattering both for the Bragg and diffuse scattering (Figs. 4*a* and 4*b*). For the 15 K data, there is good agreement in the Bragg scattering but the diffuse scattering is not fitted so well at low Q (Figs. 4*c* and 4*d*). This can be understood by examining the width, σ_L, of the approximately Lorentzian diffuse line at $Q \simeq 1.2$ Å^{-1}. $\sigma_L \simeq 0.1$ Å^{-1}, which implies that the spin disorder has a mean correlation length of $2\pi/\sigma_L \simeq 60$ Å. This is larger than the model and therefore cannot be fitted perfectly. At 200 K, we instead have $\sigma_L \simeq 0.5$ Å^{-1}, *i.e.* a correlation length of ~13 Å, well below the model size.

In order to visualize further the possibilities of the powder RMC method, we show in Fig. 5 a projection of the magnetic structure within the fitted configurations. Here the projected x axis, equivalent to the cubic $[0\bar{1}1]$ direction, is one of the principal axes of the configuration supercell. Long-range antiferromagnetic ordering is clearly visible at 15 K with consecutive (111) planes, perpendicular to the z axis, having alternate average magnetization. At 200 K, one can only recognize the lattice of atomic positions and the spins appear to be randomly oriented. Further investigation shows, however, that the fitted configurations have definite spin correlations even above 200 K. A detailed analysis and interpretation of the resulting model configurations, at

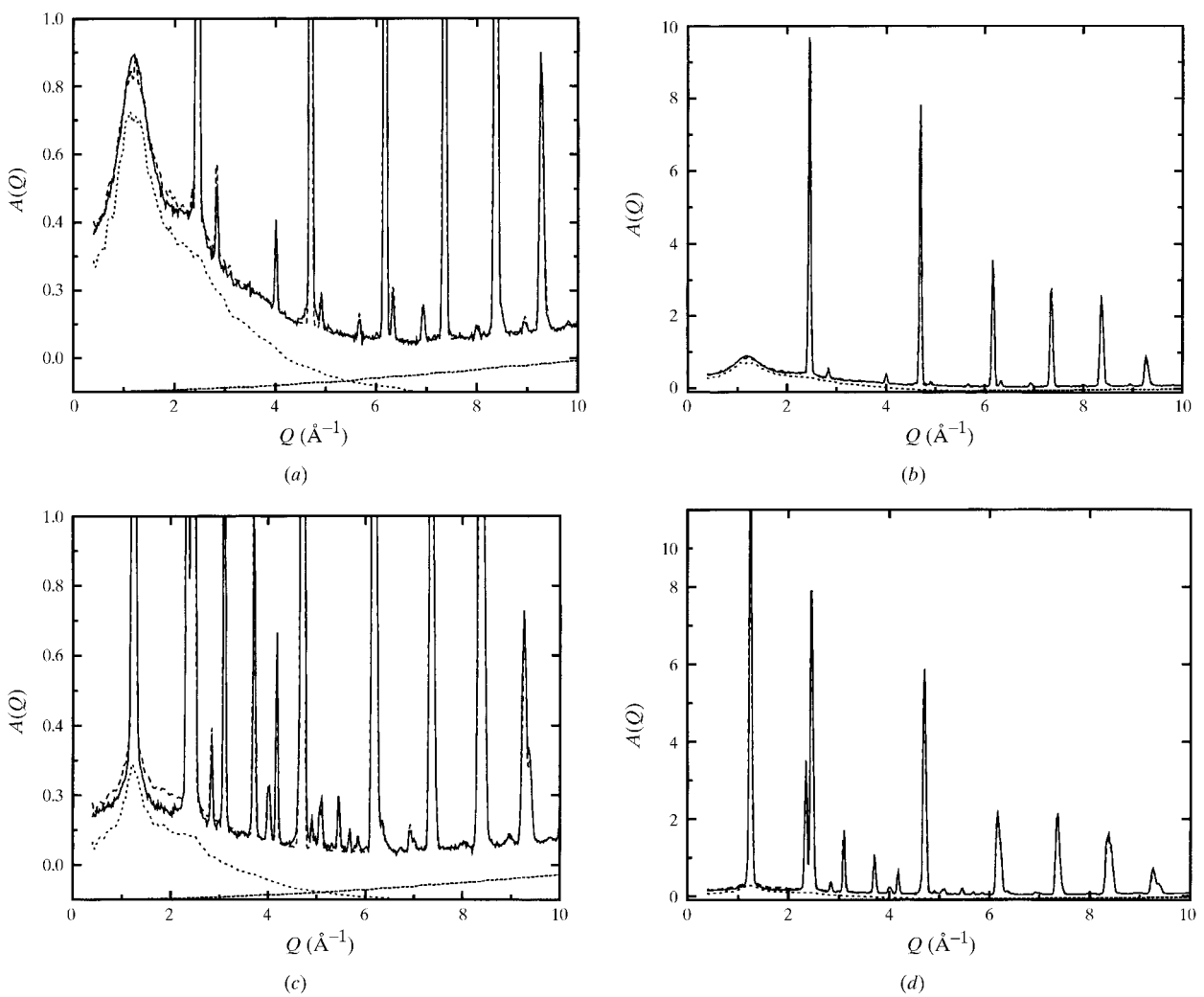

Fig. 4. Results of powder RMC modelling for MnO at (*a*), (*b*) 200 K and (*c*), (*d*) 15 K. Experimental $A(Q)$ (solid line), RMC total $A(Q)$ (dashed line) with magnetic diffuse scattering (dots) and lattice diffuse scattering (short dashes); the latter two are offset by −0.1 for clarity.

all the temperatures measured, has been presented elsewhere (Mellergård *et al.*, 1998).

6. Conclusions

We have described the modification of the direct-calculation RMC method to allow simultaneous modelling of both lattice and magnetic disorder in powder crystalline materials. The important feature of the method, compared with standard refinement techniques, is that diffuse scattering is included. All four contributions to the scattering, that is lattice Bragg and diffuse scattering and magnetic Bragg and diffuse scattering, are calculated from a single model, so it must be self-consistent. The scattering is calculated directly, including resolution, taking full advantage of the periodic boundary conditions and avoiding the truncation problems experienced with RMC transform methods. However, since the configuration is finite, we cannot reproduce any local correlations that occur on a length-scale longer than its smallest dimension. Diffuse features obviously have to be broader than the average distance between supercell reciprocal vectors in order to obtain the correct shape. The method will therefore run into problems at temperatures very close to long-range-ordering transitions, but it will still be possible to examine trends at the approach to such transitions.

The method has been shown to work successfully, as applied to MnO. The model Bragg intensity decreases properly with increasing disorder and at the same time the intensity is transferred into diffuse scattering, in good agreement with the experimental data. The scattering due to spin fluctuations around the Néel temperature is in fact fitted rather well, despite the fact that the model is of finite size. In studies of more complex transition-metal oxides, like giant magneto-resistance manganites and high-T_c superconductors, it is often a problem to isolate diffuse lattice features because of the presence of diffuse magnetic scattering, or *vice versa*. With the method described in this paper, it should be possible to extract self-consistent information from such systems. There are also, of course, many possible applications in studies of nonmagnetic systems.

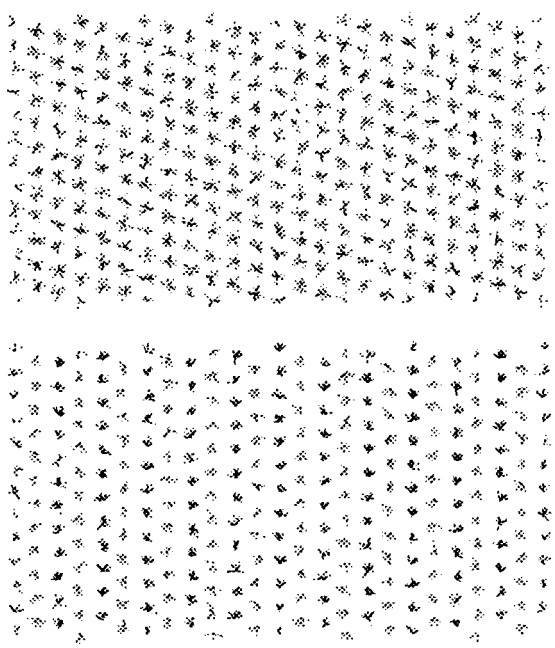

Fig. 5. Projections of the RMC spin distribution for MnO at 200 K (top) and 15 K (bottom) along the x axis of the configuration. This is the equivalent to the $(0\bar{1}1)$ plane of the cubic unit cell and the z axis is equivalent to [111]. Spin colours are chosen on a scale ranging from blue to red proportional to the value of the spin component along the cubic [110] direction, which projects onto the y axis and is the approximate average magnetization axis of the configuration at 15 K.

This work was supported by the Swedish Natural Sciences Research Council.

References

Beverley, M. N. & Nield, V. M. (1997). *J. Phys. Condens. Matter*, **9**, 5145–5156.
Keen, D. A., Hayes, W. & McGreevy, R. L. (1990). *J. Phys. Condens. Matter*, **2**, 2773–2786.
Keen, D. A., McGreevy, R. L., Bewley, R. I. & Cywinski, R. (1995). *Nucl. Instrum. Methods Phys. Res. A*, **354**, 48–52.
Lovesey, S. W. (1984). *Theory of Neutron Scattering from Condensed Matter*, Vol. I, pp 34–39, Vol. II, pp. 250–258. Oxford University Press.
McGreevy, R. L. (1994). *Mater. Sci. Forum*, **166–169**, 45–46.
Mellergård, A., McGreevy, R. L., Wannberg, A. & Trostell, B. (1998). *J. Phys. Condens. Matter*, **10**, 9401–9412.
Montfrooij, W., McGreevy, R. L., Hadfield, R. A. & Andersen, N.-H. (1996). *J. Appl. Cryst.* **29**, 285–290.
Nield, V. M., Keen, D. A., Hayes, W. & McGreevy, R. L. (1992). *J. Phys. Condens. Matter*, **4**, 6703–6714.
Nield, V. M., Keen, D. A. & McGreevy, R. L. (1995). *Acta Cryst.* A**51**, 763–771.
Proffen, T. & Welberry, T. R. (1998). *J. Appl. Cryst.* **31**, 318–326.
Pusztai, L. & McGreevy, R. L. (1997). *Physica (Utrecht)*, B**234–236**, 357–358.
Roth, W. L. (1958). *Phys. Rev.* **110**, 1333–1341.
Savitzky, A. & Golay, M. J. E. (1964). *Anal. Chem.* **36**, 1627–1639.
Soper, A. K. (1990). *Inst. Phys. Conf. Ser.* **107**, 192–196.